Applied Catalysis B: Environmental 91 (2009) 657–662

Contents lists available at ScienceDirect

Applied Catalysis B: Environmental

journal homepage: www.elsevier.com/locate/apcatb

Photo-catalytic degradation of Rhodamine B on C-, S-, N-, and Fe-doped TiO_2 under visible-light irradiation

Xiangxin Yang [a,1], Chundi Cao [a], Larry Erickson [a], Keith Hohn [a], Ronaldo Maghirang [b], Kenneth Klabunde [c,*]

[a] Department of Chemical Engineering, Kansas State University, Manhattan, KS 66506, USA
[b] Department of Biological and Agricultural Engineering, Kansas State University, Manhattan, KS 66506, USA
[c] Department of Chemistry, Kansas State University, Manhattan, KS 66506, USA

ARTICLE INFO

Article history:
Received 4 April 2009
Received in revised form 8 June 2009
Accepted 9 July 2009
Available online 17 July 2009

Keywords:
Carbon
Nitrogen
Sulfur
Iron
Dopants
TiO_2
Photocatalyst

ABSTRACT

C-, S-, N-, and Fe-doped TiO_2 photocatalysts were synthesized by a facile sol–gel method. The structure and properties of catalysts were characterized by N_2 desorption–adsorption, X-ray diffraction (XRD), UV–vis spectroscopy, and X-ray photoelectron spectroscopy (XPS). Results revealed that the surface area of the multi-doped TiO_2 was significantly increased and the crystallite size was smaller than the pure TiO_2 obtained by a similar route. Compared with TiO_2, the peak position in doped-TiO_2 XRD patterns was slightly shifted, which could be attributed to the distortion by the substitution of carbon, nitrogen, and sulfur dopants for some oxygen atoms and Fe^{3+} for Ti^{4+} in the lattice of TiO_2. These substitutions were confirmed by XPS. In addition, these dopants were responsible for narrowing the band gap of TiO_2 and shifting its optical response from ultraviolet (UV) to the visible-light region. The photocatalytic reactivities of these multi-doped TiO_2 catalysts were investigated by degrading Rhodamine B (RB) in aqueous solution under visible-light irradiation ($\lambda > 420$ nm). It was found out that the reactivity was significantly enhanced and the catalyst doped with nitrogen, carbon, sulfur, and 0.3 wt% iron had the highest photocatalytic activity.

1. Introduction

Titanium dioxide (TiO_2), as a chemically stable, nontoxic, highly efficient, and relatively inexpensive photocatalyst, has been widely used for water and air purification since many environmental pollutants can be degraded by oxidation and reduction processes on TiO_2 surface. [1–3] Under irradiation with light of sufficient energy to span TiO_2's band gap, the electron (e^-) can be promoted into the conduction band (CB), leaving a hole (h^+) in the valence band (VB). Then, electrons and holes can initiate redox reactions on the surface of TiO_2. Finally, pollutants can be degraded into CO_2 and H_2O [1]. However, the application of TiO_2 is limited by its UV activation requirement because of its large band gap (3.2 or 3.0 eV in the anatase or rutile crystalline phase, respectively). Therefore, efforts have been directed towards shifting the optical sensitivity of TiO_2 from UV to the visible-light region for the efficient use of solar energy, which is composed of only about 2–3% UV light. [4]

Transition metal dopants have been widely used to extend TiO_2's light absorption into the visible-light region. Iron is frequently employed owing to its unique half-filled electronic configuration, which might narrow the energy gap through the formation of new intermediate energy levels. [5] Choi et al. [6] studied the effects of 21 different dopants on the photoreactivity of TiO_2. Fe^{3+} dopant proved to be better than Ru^{3+}, V^{4+}, Mo^{5+}, Os^{3+}, and Re^{5+}. At 0.1–0.5 wt.%, the photocatalytic activity for the reduction of CCl_4 and the oxidation of $CHCl_3$ was significantly increased. Fe-doped TiO_2 also exhibited enhanced activity under visible-light irradiation for the degradation of methylene blue (MB), [5] methylene orange (MO), [7] methanol, [8] toluene, [9] and disinfection of E. Coli suspension. [10] It is generally accepted that the Fe^{3+} dopant formed shallow charge traps within the TiO_2 crystal lattice through the substitution of Ti^{4+}, which reduced the electron–hole recombination and improved the photocatalytic efficiency [8,11,12].

Although transition metal modified TiO_2 photocatalysts are active under visible-light irradiation, the efficiency is still low for practical use. Recently, doping nonmetal atoms, such as C, N, and S, has received much attention. Theoretical calculations showed that the p-orbitals of these dopants significantly overlapped with the valence band O 2p-orbitals, which facilitated the transport of photo-generated charge carriers to the surface of the catalyst. Wang et al. [13] reported the shift of photo response of TiO_2 from UV to the infrared region by a carbon dopant. S-doped TiO_2 showed

* Corresponding author. Fax: +1 785 532 6666.
E-mail address: kenjk@ksu.edu (K. Klabunde).
[1] Current email address: tonyjone568@yahoo.com.

0926-3373/$ – see front matter © 2009 Elsevier B.V. All rights reserved.
doi:10.1016/j.apcatb.2009.07.006

high activity for degradation of MB in water under irradiation at wavelengths longer than 440 nm. [14] Visible-light-active N-doped TiO_2 photocatalyst has been prepared by thermal nitridation of TiO_2, amination of TiO_2, sputtering, and hydrolyzing titanium-precursors in ammonia. [15–18]

It is of great interest to investigate the synergetic effects of multiple dopants on the optical shift, crystallinity, surface areas, and activity of TiO_2. It was reported that N and F co-doped TiO_2 had higher visible-light activity than N-doped or F-doped TiO_2 since N dopant improved the visible-light absorption and the doped F atom enhanced the surface acidity and the adsorption of agents. [19] Tryba [20] synthesized C and Fe co-doped TiO_2 and it showed higher activity than TiO_2 for the decomposition of phenol in multiple uses. Our previous research showed two dopants had more beneficial effects than a single one for enhancing the absorption in the visible-light region and improving the photocatalytic activity of TiO_2. [21,22] In this work, multiple dopants-modified TiO_2, namely, C, N, S, and Fe, were developed via a facile sol–gel process, which showed an enhanced activity compared to TiO_2 owing to the modification by these dopants.

2. Experimental

2.1. Catalyst synthesis

Thiourea was used as the precursor for nonmetal atoms and iron chloride as the iron precursor. These two compounds and titanium isopropoxide (97%) were purchased from Aldrich and used without further treatment. The general procedure for the preparation was as follows: First, 3.8 g thiourea was added to a beaker containing 150 mL deionized water, which was kept in a water–ice bath. While under vigorous stirring, a certain amount of iron chloride, according to the desired Fe^{3+} doping content, was added to the solution. Next, 11 mL of titanium isopropoxide was added dropwise to the aqueous solution. The mixture was stirred for 12 h and aged for 24 h. Water was removed by drying in air at 80 °C. The dried powder was ground and calcined at 500 °C in air for 2 h. Fe doping content (x) was chosen as 0, 0.1, 0.3, and 0.5 wt%, which was the mass percentage of Fe^{3+} in the titanium oxide powder (denoted as CNS–xFe–TiO_2). The same procedure, without thiourea and iron chloride, was used to prepare pure TiO_2. Commercial Degussa P25 TiO_2 (anatase/rutile = 75/25) with a specific surface area of 50 m^2/g was used for comparison purposes.

2.2. Catalyst characterization

N_2 adsorption–desorption isotherms were obtained at 77 K on a NOVA 1000 series instrument (Quantachrome, USA). The specific surface area was determined by multipoint Brunaer–Emmett–Teller (BET) method using the adsorption data in the relative pressure (P/P_0) range of 0.05–0.3. Desorption isotherms were used to determine the pore size distribution, pore volume, and pore diameter using the Barret–Joyner–Halender (BJH) method. Prior to measurements, the catalysts were degassed at 150 °C for 1 h.

X-ray diffraction (XRD) patterns were obtained with a Bruker D8 diffractometer with Cu Kα radiation (1.5406) at 40 kV and 40 mA. Measurements were recorded in steps of 0.025° with a count time of 2 s in the 2θ range of 20–65°. The phases were identified with the aid of Joint Committee on Powder Diffraction Standards (JCPDS) files.

UV–vis absorbance spectra of catalysts were recorded with a Cary 500 Scan UV–vis-NIR spectrophotometer. All spectra were referenced to poly (tetrafluoroethylene).

X-ray photoelectron spectroscopy (XPS) data were recorded using a PerkinElmer PHI 5400 electron spectrometer. The spectrometer utilizes achromatic Al Kα radiation (1486.6 eV). Before samples were tested, the spectrometer was calibrated by setting the binding energies of Au $4f_{7/2}$ and Cu $2p_{3/2}$ to 84.0 and 932.7 eV, respectively. Binding energies for the samples were normalized with respect to the position of the C 1s peak resulting from adsorbed hydrocarbon fragment. The XPS binding energies were measured with a precision of 0.1 eV.

2.3. Photocatalytic activity measurements

The photocatalytic activity of catalysts was evaluated by the degradation of Rhodamine B (RB) in an aqueous solution. The light source was a 1000 W high-pressure Hg arc lamp (Oriel Corporation). The combination of a vis-NIR long pass filter (400 nm) and colored glass filter (>420 nm) was used to eliminate UV radiation during visible-light experiments. A general procedure was carried out as follows: First, 100 mL aqueous RB solution (1×10^{-5} mol/L) was placed in a water-jacketed reactor, which was maintained at a temperature of 25 °C. Then, 30 mg catalyst was suspended in the solution. The suspension was stirred vigorously for 60 min in the dark to establish adsorption–desorption equilibrium of RB. The suspension was then irradiated under visible-light. Samples were withdrawn periodically from the reactor, then centrifuged and analysed by recording variations in the absorption in the UV–vis spectra of RB using a Cary 500 UV–vis spectrophotometer at its characteristic wavelength (λ = 553 nm). [23–25] The reproducibility of the results was checked by repeating the results at least three times and was found to be within acceptable limits (±1%).

3. Results and discussion

3.1. N_2 adsorption–desorption

Fig. 1 illustrates N_2 adsorption–desorption isotherms and pore size distribution of CNS-xFe-TiO_2 catalysts. All samples showed isotherms of type IV with an H2 hysteresis loop, indicating the mesoporous nature, attributed to the aggregation of TiO_2 crystallites. [26] The BJH analysis yielded a peak at a pore diameter of 5.2 nm for TiO_2 and 5.7 nm for CNS-xFe-TiO_2, suggesting a very narrow distribution of the mesopore dimensions. Table 1 summarizes the surface area, pore volume, and pore diameter of the catalysts. The CNS-0Fe-TiO_2 exhibited much higher surface area, pore volume, and pore diameter than pure TiO_2. Apparently, these nonmetal atom dopants prevented the aggregation of smaller crystallites, forming larger pores and increasing surface areas. Another remarkable phenomenon was that the addition of an iron dopant further increased the surface area slightly. The beneficial effect of the iron dopant was attributed to the enhanced lattice strain because of the iron incorporation into the TiO_2 network and then decreased grain growth rate, i.e., sintering [5,27]. The incorporation of these dopants was further confirmed by later XRD analysis.

3.2. UV–vis spectroscopy

Fig. 2 shows UV–vis diffuse reflectance spectra of the pure and doped-TiO_2. As expected, pure TiO_2 showed absorption only in the UV region (less than 400 nm), due to the intrinsic band gap absorption of TiO_2. The onset of the absorption spectrum of CNS-xFe-TiO_2 was shifted towards visible-light, a result of carbon, nitrogen, sulfur, and iron dopants. It has been reported that when O atom of the TiO_2 lattice was substituted by C, N, or S, the p-orbital of these dopants overlapped with the valence band O 2p-orbitals. [17,28]. Therefore, the band gap of TiO_2 became narrower and the absorption edge shifted to the lower energy. In addition, elemental carbon or carbonaceous species could act as photosensitizer and effectively extend the absorption to visible-light region [21,22,29].

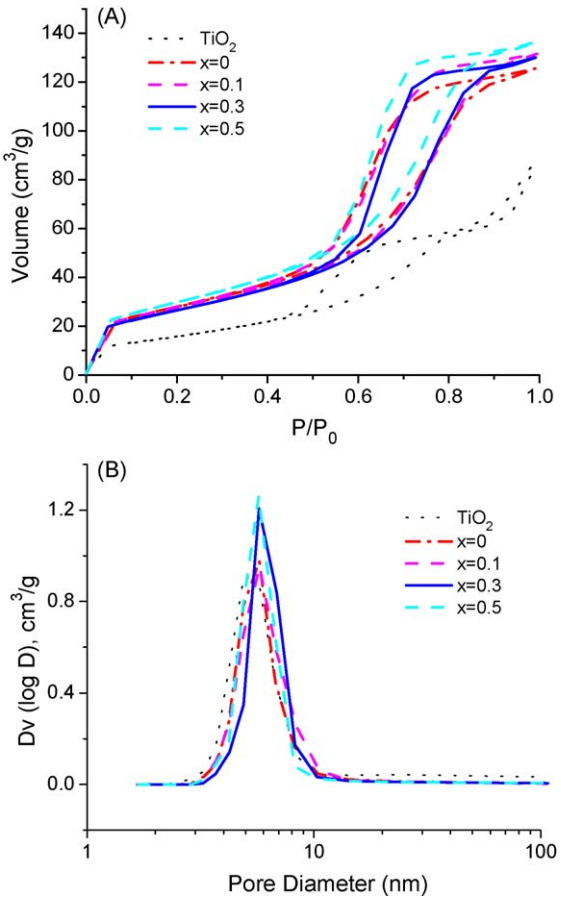

Fig. 1. N2 adsorption–desorption isotherms (A) and pore size distribution (B) of pure TiO_2 and CNS-*x*Fe-TiO_2 catalysts.

Table 1
Textural property of catalysts.

Catalyst	Surface area (m^2/g)	Pore volume (cm^3/g)	Pore diameter (nm)	Crystallite size (nm)
TiO_2	57	0.14	4.2	14.0
CNS-0Fe-TiO_2	96	0.21	5.74	9.3
CNS-0.1Fe-TiO_2	98	0.22	5.75	8.9
CNS-0.3Fe-TiO_2	100	0.22	5.72	8.9
CNS-0.5Fe-TiO_2	103	0.23	5.71	9.0

With the addition of Fe^{3+}, the absorbance in the visible-light range was enhanced, which can be attributed to the interaction between Fe^{3+} d electrons and the TiO_2 conduction or valence band since the Fe dopant could introduce impurity levels within the band gap of TiO_2. [30] The electronic transitions between the impurity level and the valence or conduction band effectively red shifted the band edge absorption threshold. [31] The absorption edge shift from UV to the visible-light region apparently indicates there is smaller band gap energy for CNS-*x*Fe-TiO_2 catalysts.

3.3. X-ray diffraction

Fig. 3 exhibits the XRD patterns of pure and doped-TiO_2. The characteristic (1 0 1) plane diffraction peak ($2\theta = 25.3^\circ$) of anatase phase is clearly observed. No peaks for the other TiO_2 phases (rutile or brookite) appear. For CNS-0Fe-TiO_2, the width of this peak broadened and its intensity was significantly decreased. With the addition of iron, this phenomenon was further enhanced. The average crystallite size was estimated by

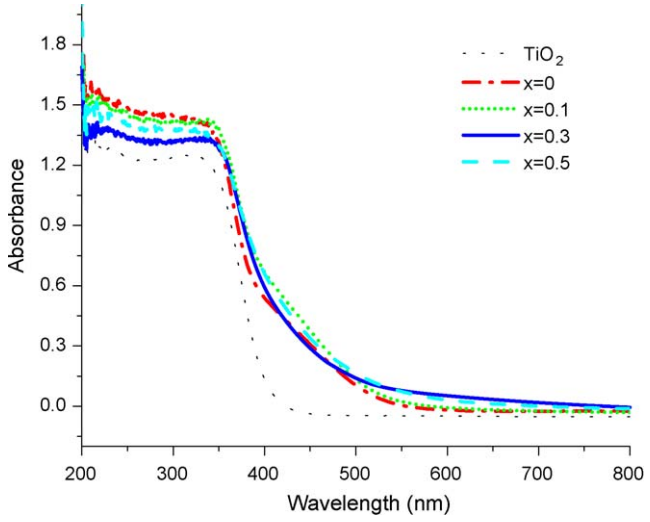

Fig. 2. The UV diffuse reflectance spectra of pure TiO_2 and CNS-*x*Fe-TiO_2 catalysts.

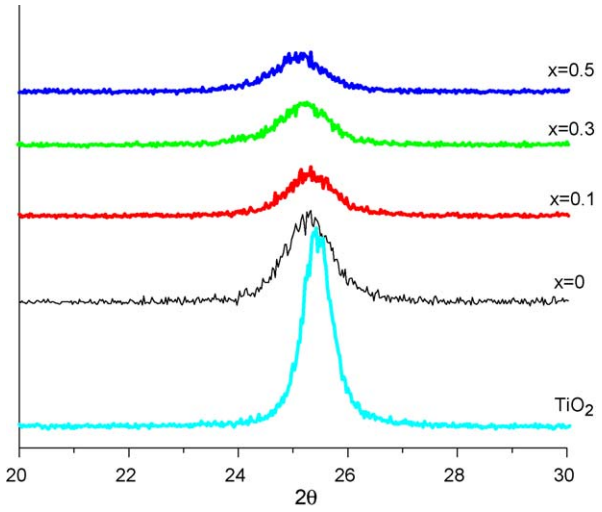

Fig. 3. XRD patterns of pure TiO2 and CNS-*x*Fe-TiO2 catalysts.

the Scherrer equation ($d = 0.94\lambda/\beta\cos\theta$, where λ was the X-ray wavelength, β was the full width at half maximum of the (1 0 1) peak, and θ was the half angle of the diffraction peak on the 2θ scale). The calculated crystallite size was listed in Table 1. It was obvious that the crystal growth was significantly suppressed by these dopants, consistent with N_2 desorption–adsorption results. The effect of nonmetal dopants was more remarkable than that of the iron dopant. With the introduction of iron, the further decrease in crystallite size can be ascribed to the retarding effect of Fe^{3+} on TiO_2 anatase crystallite growth, which favored the formation of smaller TiO_2 crystallites [27]. We also noticed that for the (1 0 1) plane peak, a small shift occurred in the peak position after the introduction of C, N, and S. Therefore, the crystal lattice was distorted by these dopants. Since the radii of Fe^{3+} and Ti^{4+} for coordination number of 6 were 0.79 and 0.75 Å, respectively, the substitution of Ti^{4+} site by Fe^{3+} ion should be facile without a significant crystalline distortion [6,32]. The replacement of Ti^{4+} by Fe^{3+} was proven by the further slight shift of the (1 0 1) peak with iron introduction. Although the Fe ion content in our samples was increased up to 0.5 wt%, no other crystalline phase (Fe_2O_3 or Fe_xTiO_y) could be found. We assumed that iron ions were incorporated into the TiO_2 network (replacing Ti^{4+} or locating at interstitial sites) or well dispersed on the surface.

3.4. X-ray photoelectron spectroscopy

To investigate the chemical states of dopants in TiO_2, C 1s, N 1s, S 2p, and Fe 2p core levels were measured by XPS. C 1s, N 1s, and S 2p XPS spectra of CNS-0Fe-TiO_2 and Fe 2p of CNS-0.3Fe-TiO_2 are shown in Fig. 4.

The C 1s XPS spectra showed a strong peak at 285 eV and a shoulder at around 288 eV. After sputtering, a new peak appeared at 281 eV. Three forms of carbon species have been previously detected: elemental carbon with binding energy of 285 eV; surface-adsorbed carbonate species (288 V); Ti–C bond resulting from substituting the lattice oxygen atoms by carbon (281 eV) [13,33]. Therefore, multiple carbon species, namely, substitutional and interstitial carbon atoms and carbonate species, existed in the lattice of TiO_2.

The S 2p XPS spectrum showed a peak at 168 eV. The assignment of this peak was controversial. A broad peak attributed to S $2p_{3/2}$ at around 168 eV suggested several oxidation states of S atoms: the peak of the S^{6+} state appeared at 168.2 eV and the peak at 167.5 eV was assigned to S^{4+}. [34] However, it was also reported that when SO_2 molecules were adsorbed on a TiO_2 surface, the peak of the S 2p state was in the region of 166–170 eV. [35] The controversy was likely due to different preparation methods or post treatments. It was more reasonable to attribute this peak to S^{6+} state in our case since we treated the sample in air at 500?C for 2 h. After sputtering, a new peak appeared at 160.2 eV, indicating that sulfur entered the lattice of TiO_2 and substituted for oxygen atoms.

The N 1s XPS spectrum showed a very broad peak between 398 and 402 eV. Peaks in this region were assigned to chemisorbed N_2 molecules and/or N-containing compounds, such as NO_x or NH_3 formed during the decomposition and oxidation of the N-precursors. [36,37] After sputtering, the broad peak disappeared and a new one was observed at around 396 eV, which usually has been assigned to N^{2-} anions resulting from substitution for oxygen sites by nitrogen atoms in the TiO_2 lattice. [38]

The Fe 2P XPS spectrum showed a peak at 709.1 eV. The peak can be assigned to Fe^{3+}. [39,40] The spectra pre and after sputtering were nearly identical, indicating Fe^{3+} existed both on the surface and inside the bulk of TiO_2 powder.

Based on XPS survey spectra after sputtering of CNS-0Fe-TiO_2 and CNS-*x*Fe-TiO_2 (not shown here), the atomic concentration of C, N, and S were 6.3, 0.2, and 1.8%, respectively. The further addition of iron dopant did not obviously affect the concentration of sulfur and nitrogen, while the carbon content decreased some. At this point, we have not further studied this phenomenon.

3.5. Degradation of RB

Characterization results indicate that the optical response of TiO_2 was shifted from UV to visible-light region with the introduction of carbon, nitrogen, sulfur, and iron dopants. This implied that these multi-doped TiO_2 catalysts, unlike pure TiO_2, might be very active under visible-light irradiation. The investigation of visible-light-activity was carried out by the degradation of RB in an aqueous solution. For the comparison of reaction rate among different catalysts, pseudo-first-order reaction equation was introduced as follows:

$$\frac{-dC}{dt} = kC \quad (1)$$

where C is the RB concentration at time t and k is the apparent reaction rate constant.This equation can be integrated to give the following form:

$$-\ln\left(\frac{C}{C_0}\right) = kt \quad (2)$$

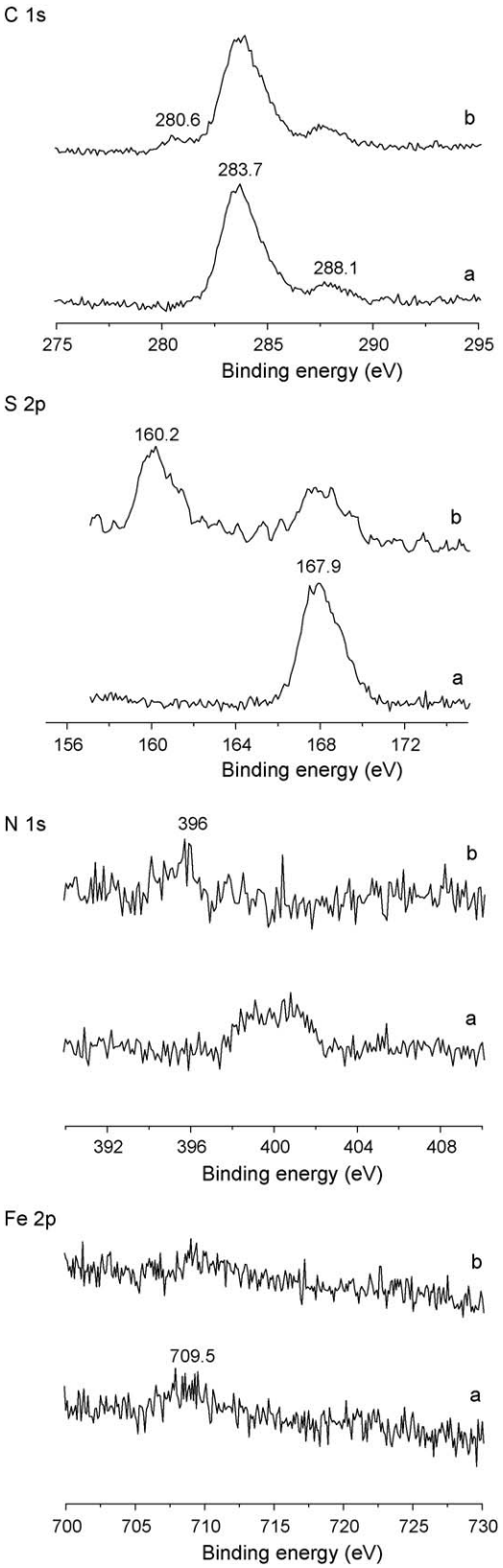

Fig. 4. XPS spectra for the C 1s, N 1s, S 2p core levels of CNS-0Fe-TiO2 and Fe 2p of CNS-0.3Fe-TiO2 (a: before sputtering; b: after sputtering).

This kinetic model has been successfully applied to various heterogeneous photocatalytic liquid–solid systems, such as Fe(III)-doped TiO_2/methyl orange [41] and anion-doped TiO_2/methylene blue. [42] According to Beer's law, the absorbance at

553 nm (the characteristic absorption wavelength of RB) was proportional to the concentration of RB in the reaction solution, so $\ln(C/C_0)$ equaled $\ln(A/A_0)$, where A_0 was the solution absorbance at time zero and A was the solution absorbance at a time t after turning on the lamp. It should be pointed out that the concentration of RB in the aqueous solution decreased before lighting because of adsorption in the dark: the values were 6.8, 7.5, 9.4, 9.4, 9.6, and 9.8% of original RB concentration for P25, TiO_2 and CNS-xFe-TiO_2 with x equals 0, 0.1, 0.3, and 0.5, respectively. Most of the concentration decrease occurred during irradiation, therefore, the decrease in RB concentration during irradiation was due to chemical reaction rather than adsorption. For convenience, we assumed that the concentration of RB after desorption–adsorption equilibrium was the initial concentration, C_0. Fig. 5 shows the degradation of RB as a function of reaction time in the presence of different catalysts under visible-light irradiation. According to the above kinetic model, the rate constants k were found to be 0.0010, 0.0016, 0.0029, and 0.0019 min^{-1} for CNS-xFe-TiO_2 with x equals 0, 0.1, 0.3, and 0.5, respectively, while k for pure TiO_2 was 0.0002 min^{-1} and 0.00016 min^{-1} for P25. Therefore, the visible-light reactivity of TiO_2 was significantly enhanced with these dopants, especially for CNS-0.3Fe-TiO_2 catalyst. The small but not negligible activity of pure TiO_2 and Degussa P25 was attributed to the self-photosensitized process. [43] After absorbing light, the excited dyes such as Rhodamine B injected an electron into the conduction band of TiO_2 where it was captured by surface-adsorbed O_2 to form $O_2^{\bullet-}$, and then, the dye cation radicals were degraded via attack by oxygen active species. However, the efficiency was very low because of the fairly slow interfacial electron transfer rate [43,44]. In addition, it was noticed that the degradation of RB did not occur in the absence of catalysts or visible-light under the experimental conditions.

In order to explain the enhanced visible-light-activity of these multi-doped TiO_2, several possible mechanisms were proposed. As shown in Fig. 6, with the substitution for oxygen atoms by nonmetal atoms (carbon, nitrogen, and sulfur) and Ti^{4+} by Fe^{3+} in the crystal structure of TiO_2, new impurity levels are introduced between the conduction and valence band of TiO_2, then the electrons can be promoted to the conduction band from these impurity levels. The electrons can also be promoted from the valence band to another impurity level introduced by iron dopant, or from the lower to the higher impurity levels. Therefore, doped CNS-xFe-TiO_2 photocatalysts have narrower band gap than pure TiO_2 and could increase the absorption in the visible-light region. Subsequently, the departed electrons and holes migrate to the surface of catalysts and react with adsorbed O_2 and H_2O, respectively, forming $O_2^{\bullet-}$ and $OH^{\bullet}$, the main species responsible for the degradation of pollutants, such as RB in our case. With the addition of iron dopant, the reactivity of the catalyst is further increased. However, the reactivity decreases dramatically when x is increased from 0.3 to 0.5 wt%, indicating there is an optimal concentration of iron dopant. This is consistent with published data: [12] at concentration below the optimal value (0.3 wt% in our case), there are fewer trapping sites available and Fe^{3+} serves as shallow trapping sites for charge carrier (e^- or h^+), thereby separating the arrival time of e^- and h^+ at the surface and increasing the efficiency. At high concentration, these trapped e^- or h^+ might recombine together before migrating to the surface, resulting in lower photocatalytic activity of TiO_2. Thus, the efficiency is strongly associated with Fe^{3+} concentration. The optimal Fe^{3+} dopant concentration in our case is not consistent with others, which might be related to different preparation methods, particle size, multiple dopants effect, or model compounds. The second mechanism is related with doped elemental carbon or carbonaceous species which could act as photosensitizer [21,22]. As shown in Fig. 7, under irradiation of visible-light, the excited photosensitizer injects electrons into the conduction band. The electrons could be further transferred to surface-adsorbed oxygen molecules and form $O_2^{\bullet-}$ and initiats the degradation of RB. Although this mechanism is similar to the dye self-photosensitized process we previously mentioned during the discussion of very low visible-light activity of pure TiO_2 or Degussa P25, its photo-efficiency should be higher because of higher interfacial electron transfer rate since it is the excited sensitizer rather than dye itself that injects an electron into the conduction band of TiO_2 after absorbing light. It was commonly accepted that dye was the only light absorbing species in self-photosensitized process [43].

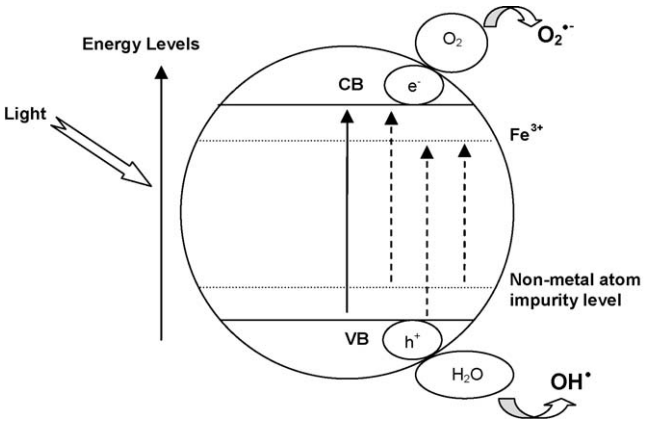

Fig. 6. Schematic diagram of doped-TiO2 and initial redox process after activation by light.

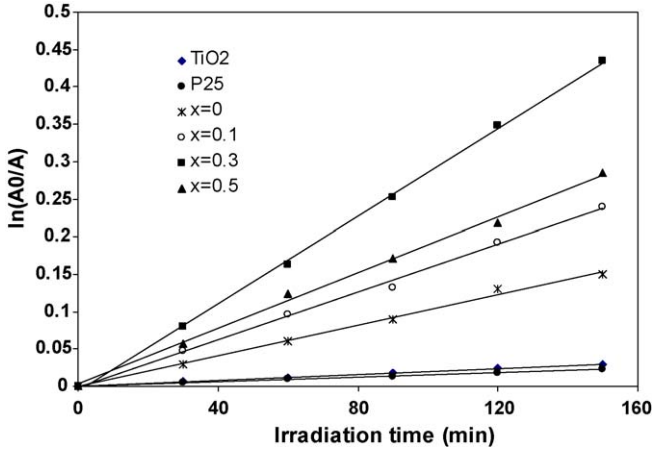

Fig. 5. The degradation of RB using different catalysts under visible-light irradiation.

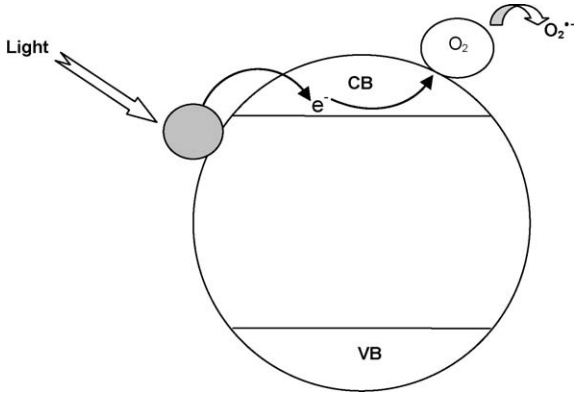

Fig. 7. Schematic diagram of photosensitizer-TiO2 system and initial redox process after activation by light.

4. Conclusions

In this research, we successfully prepared multi-doped TiO_2 photocatalysts with anatase structure. These multi-dopants, namely, carbon, nitrogen, sulfur, and iron retarded the growth and aggregation of TiO_2 particles. Multiple carbon species, substitutional and interstitial carbon atoms and carbonate species, were found in the lattice of TiO_2. Nitrogen and sulfur atoms were incorporated into the lattice of TiO_2 and existed in the state of S^{2-} and N^{2-}, respectively, and iron dopant existed as Fe^{3+}. These incorporations were verified by XPS and XRD analyses. The diffuse reflectance spectra suggested the photo absorption of multi-doped TiO_2 was extended to the visible-light region. It was assumed that these dopants introduced impurity levels between the conduction and valence band of TiO_2, leading to narrower band gap and enhancing the visible-light absorption. Compared with TiO_2, these catalysts showed much higher activity for the degradation of RB under visible-light irradiation. Several possible mechanisms were proposed for the improvement of visible-light reactivity of multi-doped TiO_2.

Acknowledgements

This work was supported by Army Research Office (through DTRA contract SPO-AA06SP0012), the NanoScale Corporation, and the Kansas State University Targeted Excellence Program.

References

[1] X. Chen, S. Mao, Chem. Rev. 107 (2007) 2891.
[2] M. Hoffmann, S. Martin, W. Chen, D. Bahnemannt, Chem. Rev. 95 (1995) 69.
[3] A. Linsebigler, G. Lu, J. Yates Jr., Chem. Rev. 95 (1995) 735.
[4] T. Ohno, J Jpn. Pet. Inst. 49 (2006) 168.
[5] J. Zhu, J. Ren, Y. Huo, Z. Bian, H. Li, J. Phys. Chem. C 111 (2007) 18965.
[6] W. Choi, A. Termin, M.R. Hoffmann, J. Phys. Chem. 98 (1994) 13669.
[7] X. Zhang, L. Lei, Mater. Lett. 62 (2008) 895.
[8] C. Wang, D. Bahnemannt, J. Dohrmann, Chem. Commun. 16 (2000) 1539.
[9] E. Butler, A. Davis, J. Photochem. Photobiol. A 70 (1993) 273.
[10] T. Egerton, A. Kosa, P. Christensen, Phys. Chem. Chem. Phys. 8 (2006) 398.
[11] C. Wang, Q. Li, R. Wang, J. Mater. Sci. 39 (2004) 1899.
[12] Z. Zhang, C. Wang, R. Zakaria, J. Ying, J. Phys. Chem. B 102 (1998) 10871.
[13] X. Wang, S. Meng, X. Zhang, H. Wang, W. Zhang, Q. Du, Chem. Phys. Lett. 444 (2007) 292.
[14] T. Ohno, T. Mitsui, M. Matsumura, Chem. Lett. 32 (2003) 364.
[15] H. Chen, A. Nambu, W. Wen, J. Graciani, Z. Zhong, J. Hanson, E. Fujita, J. Rodriguez, J. Phys. Chem. C 111 (2007) 1366.
[16] C. Burda, Y. Lou, X. Chen, A.C.S. Samia, J. Stout, J.L. Gole, Nano Lett. 3 (2003) 1049.
[17] R. Asahi, T. Morikawa, T. Ohwaki, K. Aoki, Y. Taga, Science 293 (2001) 269.
[18] T. Ihara, M. Miyoshi, Y. Iriyama, O. Matsumoto, S. Sugihara, Appl. Catal. B: Environ. 42 (2003) 403.
[19] D. Li, N. Ohashi, S. Hishita, T. Kolodiazhnyi, H. Haneda, J. Solid State Chem. 178 (2005) 3293.
[20] B. Tryba, J. Hazard. Mater. 151 (2008) 623.
[21] X. Yang, C. Cao, K. Hohn, L. Erickson, R. Maghirang, K. Klabunde, J. Catal. 252 (2007) 296.
[22] X. Yang, C. Cao, L. Erickson, K. Hohn, R. Maghirang, K. Klabunde, J. Catal. 260 (2008) 128.
[23] E. Soares, M. Lansarin, C. Moro, Brazilian J. Chem. Eng. 24 (2007) 29.
[24] K. Byrappa, A. Subramani, S. Ananda, K. Rai, R. Dinesh, M. Yoshimura, Bull. Mater. Sci. 29 (2006) 433.
[25] F. Chen, J. Zhao, H. Hidaka, Int. J. Photoenergy 5 (2003) 209.
[26] M. Rahman, K. Krishna, T. Soga, T. Jimbo, M. Umeno, J. Phys. Chem. Solids 60 (1999) 201.
[27] Y. Zhang, A. Reller, J. Mater. Chem. 11 (2001) 2537.
[28] C. Enache, J. Schoonman, R. Krol, J. Electroceram. 13 (2004) 177.
[29] C. Lettmann, K. Hildenbrand, H. Kisch, W. Macyk, W. Maier, Appl. Catal. B: Environ. 32 (2001) 215.
[30] Y. Cong, J. Zhang, F. Chen, M. Anpo, D. He, J. Phys. Chem. C 111 (2007) 10618.
[31] M. Litter, J. Navio, J. Photochem. Photobiol. A 98 (1996) 171.
[32] M.S. Nahar, K. Hasegwa, S. Kagaya, Chemosphere 65 (2006) 1976.
[33] Z. Shi, X. Ye, K. Liang, S. Gu, F. Pan, J. Mater. Sci. 22 (2003) 1255.
[34] T. Ohno, T. Tsubota, K. Nishijima, Z. Miyamoto, Chem. Lett. 33 (2004) 750.
[35] D.I. Sayago, P. Serrano, O. Bohme, A. Goldoni, G. Paolucci, E. Roman, J.A. Martin-Gago, Phys. Rev. B 64 (2001) 205402.
[36] N.C. Saha, H.G. Tompkins, J. Appl. Phys. 72 (1992) 3072.
[37] D. Li, N. Ohashi, S. Hishita, T. Kolodiazhnyi, H. Handea, J Solid State Chem. 178 (2005) 3293.
[38] H. Irie, Y. Watanabe, K. Hashimoto, J. Phys. Chem. B 107 (2003) 5483.
[39] X. Shen, J. Guo, Z. Liu, S. Xie, Appl. Surf. Sci. 254 (2008) 4726.
[40] M. Zhou, J. Yu, B. Cheng, J. Hazard. Mater. B 137 (2006) 1838.
[41] X. Wang, J. Li, H. Kamiyama, Y. Moriyoshi, T. Ishigaki, J. Phys. Chem. B 110 (2006) 6804.
[42] G. Li, L. Chen, N. Dimitrijevic, K. Gray, Chem. Phys. Lett. 451 (2008) 75.
[43] C. Chen, W. Zhao, J. Li, J. Zhao, Environ. Sci. Technol. 36 (2002) 3604.
[44] H. Fu, C. Pan, W. Yao, Y. Zhu, J. Phys. Chem. B 109 (2005) 22432.